Chemical Physics Letters 592 (2014) 211–216

Contents lists available at ScienceDirect

Chemical Physics Letters

journal homepage: www.elsevier.com/locate/cplett

# Quadrupole ion trap/time-of-flight photo-fragmentation spectrometry of the hexa-*peri*-hexabenzocoronene (HBC) cation

J. Zhen [a,b,*], D.M. Paardekooper [a], A. Candian [b], H. Linnartz [a], A.G.G.M. Tielens [b]

[a] Sackler Laboratory for Astrophysics, Leiden Observatory, University of Leiden, PO Box 9513, NL 2300 RA Leiden, The Netherlands
[b] Leiden Observatory, University of Leiden, PO Box 9513, NL 2300 RA Leiden, The Netherlands

ARTICLE INFO

*Article history:*
Received 11 June 2013
In final form 3 December 2013
Available online 22 December 2013

ABSTRACT

We have studied the photo-fragmentation of the HBC cation $-C_{42}H_{18}^{+}-$ a large PAH cation of potential astrophysical interest. HBC cation photo-fragment patterns are measured upon irradiation by an unfocused Nd:YAG laser (532 nm) for different experimental conditions, using quadrupole ion trap, time-of-flight mass spectrometry. Both stepwise dehydrogenation of $C_{42}H_{18}^{+}$ and $C_2/C_2H_2$ loss pathways are identified as relevant photodissociation routes.



## 1. Introduction

Polycyclic aromatic hydrocarbons, PAHs, both neutral and charged, are likely the molecular species responsible for the mid-IR emission features (strongest at 3.3, 6.2, 7.7, 8.6, and 11.2 μm) detected from a variety of astrophysical objects. These emissions are expected to occur following internal energy redistribution after UV excitation by photons arising from the interstellar radiation field [1–6]. PAHs in the interstellar medium (ISM) are expected to be large, with 30 up to 100 carbon atoms species responsible for most of the mid-IR emission, and carrying as much as 10–15% of the elemental carbon [4]. The observed spectra imply that a considerable fraction of interstellar PAHs are ionized [7,8], consistent with the fact that their ionization potential is generally well below the energy of the available photons, and this photo-ionization plays a key role in the energy balance of gas in the ISM [9,10].

Photo-fragmentation is one of the main destruction pathways for PAHs in space [4]. In order to understand PAH-cation dissociation dynamics, dedicated laboratory studies are needed that characterize fragmentation patterns upon photo-excitation, and their dependence on, e.g., wavelength and photon intensity. A number of experiments have studied the photo-chemistry of (small) PAHs (see for example [11,12]). Experimental studies of species relevant to astronomy have generally used a time-of-flight, photo-ionization mass spectrometry (PIMS) technique, focusing on the appearance (internal) energy at which the dissociation rate is approximately $10^4\ s^{-1}$ (e.g., an experimental timescale of $10^{-4}$ s; [13,14]). In these studies, loss channel(s) mainly involve (sequential) hydrogen loss but $C_2H_2$ (and $C_2H_3$) loss is also observed at higher internal energies. In the ISM, however, different molecular dynamical timescales are at play. Fragmentation has to compete with relaxation through IR emission that occurs on time scales of the order of ~0.01–1 s, depending on the size of the species [10,15]. In addition, since PAHs typically absorb $\sim 10^8$ UV photons over their lifetime – some 100 Myr – even dissociation channels with a low probability are relevant [10]. Moreover, astrochemically related studies focus on the smaller PAHs (Naphthalene to Coronene with 10–24 C-atoms) [4,13,16] that may be less abundant in space.

We have studied the long time-scale, i.e., multi-second photostability of the large PAH cation hexa-*peri*-hexabenzocoronene (HBC) cation. HBC ($C_{42}H_{18}$) is a large all-benzenoid PAH which has been suggested to be present in space [17–19] and that is taken here as a prototypical example for large(r) PAHs.

## 2. Experiment

The experiments are performed on the 'instrument for Photodynamics of PAHs' (i-PoP; Figure 1), consisting of two differentially pumped chambers. The source chamber (QIT chamber) comprises a commercially available quadrupole ion trap (Jordan C-1251) that is connected via a 2 mm skimmer to the detection chamber (TOF chamber) with a time-of flight mass spectrometer (Jordan D-850). The base pressure of the two chambers is $\sim 5.0 \times 10^{-8}$ mbar (QIT) and $\sim 2.0 \times 10^{-8}$ mbar (TOF). HBC is evaporated in the source chamber by heating the powder (Kentax) with purity better than 99.5% in an oven (Heat Wave Labs) at a temperature of 570 K. Subsequently, evaporated molecules are ionized by an electron gun (EGUN, Jordan C-950) and transported into the ion trap via an ion gate. The method follows standard (gating) procedures, using plates on different potentials and a split Einzel lens. A DC voltage pulser (Jordan D-1040) controls the opening and closing of the gate and typical ramp times in the trap amount to 10 ns rise time.

* Corresponding author at: Sackler Laboratory for Astrophysics, Leiden Observatory, University of Leiden, PO Box 9513, NL 2300 RA Leiden, The Netherlands. Fax: +31 (0)71 5275819.
*E-mail address:* zhen@strw.leidenuniv.nl (J. Zhen).

0009-2614/$ - see front matter © 2013 Elsevier B.V. All rights reserved.
http://dx.doi.org/10.1016/j.cplett.2013.12.005

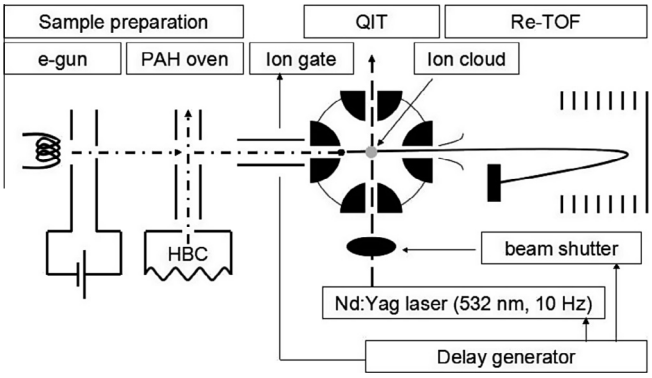


**Figure 1.** A schematic of the i-PoP setup.

Prior to ion injection, He buffer gas is introduced into the trap via a leak valve. The buffer gas pressure inside the trap is higher than the background pressure of the QIT chamber because of the conductance-limited pumping efficiency of gas out of the trap. The conductance through all the apertures of the QIT is determined as 8.34 L/s from other reported trap conductance measurements [20]. The conductance of the turbo pump for the QIT chamber is 230 L/s, so we estimate that the buffer gas pressure in the ion trap is $\sim 7 \times 10^{-6}$ mbar, with an estimated absolute uncertainty of 50%. As a result of thermalization, the PAH ions will concentrate in the center of the trap [20,21]. The ion cloud is expected to remain at a constant diameter (about 0.5 mm) in the center of the trap throughout the irradiation period. The working pressures in QIT and TOF chamber are $\sim 3.0 \times 10^{-7}$ and $\sim 3.0 \times 10^{-8}$ mbar, respectively, corresponding to a mean free path of ~300 and ~3000 m, and to ~1 and ~10 s between collisions.

The second harmonic of a Nd:YAG laser (DCR-3, Spectra-Physics) – 532 nm, ~6 ns – operated at 10 Hz is used to irradiate the trapped ions. The spatial profile of the laser beam is nearly GAUSSIAN with low intensity modulation and harmonic conversion efficiencies are high while retaining good spatial mode. The beam diameter is 7 mm; the beam divergence is 0.5 mrad, and the laser beam has a high on-axis energy density at long distance from the laser. Optical access to the QIT is realized through a 2.4 mm aperture in the ring electrode. In our experiment, the laser beam is guided horizontally through the ion trap. In addition, the intensity of the fragments of HBC cations is used in helping to align the laser beam. The laser pulse energy is measured by a power meter (Vector, H310) before the beam enters the vacuum chamber and is typically up to 18 mJ/pulse with an average power values that range up to $3.0 \times 10^6$ W. i-PoP operates at a typical frequency of 0.2 Hz, i.e., one full measuring cycle lasts 5 s. It is possible to accumulate photo-fragmentation products of multiple laser shots, thereby increasing the fragmentation yield. Experiments are usually performed during a 1.8 s slot using 18 laser shots. A beam shutter acts as a physical shield and determines the interaction time of the light with the trapped ions. The electromechanical shutter (Thorlabs SC05) is externally triggered to guarantee that the ion cloud is irradiated only for a specified amount of time during each scan cycle. The QIT rf power supply (Jordan D-1203) maintained at 3250 $V_{p\text{-}p}$ is capable of switches off the rf amplitude within two cycles. Following a ring-down of this voltage, the fragments remain in the QIT until extraction into the TOF drift tube. During ion extraction from the trap, pulsed voltages from ground to +800 V and from ground to −800V (5 ns rise-time, 10 μs width) are put onto the two end caps (Jordan D-1050) to empty the trap and transfer the ion cloud into the TOF mass spectrometer for mass analysis. The ion cloud passes a 2 mm skimmer and is then uniformly accelerated into the field-free region by a mesh at the entrance of the TOF chamber. The TOF ion signal is detected by a multi-channel plate (Jordan, C-701). The estimated total signal gain through the acquisition electronics is $2 \times 10^8$. The TOF mass spectrometer allows for simultaneous detection of the parent ion and the fragment ion signals.

A high precision delay generator (SRS DG535) controls the full timing sequence. Each scan cycle begins with an empty ion trap. At the leading edge of the master trigger the ion gate opens, allowing the ion trap to fill for a certain amount of time (typically ~3 s) with PAH ions. After a short time delay (typically ~0.2 s), the ion cloud thermalizes to room temperature (~298 K) by collisions with the He buffer gas, and as a direct consequence the diameter of the cloud shrinks [20,21]. The laser beam shutter opens and the ion cloud is irradiated. During each cycle, the laser irradiation time is changed to one of the preprogrammed time periods. At the end of the irradiation, a negative square pulse is applied to the end cap, accelerating the ions out of the trap and into the field-free TOF region the resulting mass fragments are measured. The full data-acquisition is controlled by LABVIEW routines.

In all experiments, uncertainties include the total number of ions in the trap which we estimated from the repeated blank shots, (~4%), the laser pulse energy (estimated at ~2–5% at different laser pulse energies), and the local baseline determination that results in relative abundance uncertainties of up to ~2%. Thus, the formation yield of products has a total estimated uncertainty of ~6%.

## 3. Results and discussion

The application of i-PoP to astrophysically relevant large PAHs is illustrated by the trapping efficiency and photo-dynamics of hexa-*peri*-hexabenzocoronene (HBC) cations (the $m/z$ of $^{12}C_{42}H_{18}^+$ = 522.141) following unfocused 532 nm laser irradiation. In Figure 2A a typical TOF mass spectrum is shown for a 3.0 s long filling of the trap with HBC cations. The isotopologues and HBC fragments are labeled in the inset mass spectra that are illustrative for the level of accuracy that can be achieved. In order to obtain this signal-to-noise ratio, mass-spectra are averaged 150 times. The mass resolution of the spectrometer is determined at around 1500. The measured mass spectra in the range $m/z$, 522–526, corresponding to isotopologues $^{12}C_{42}H_{18}^+$ (62.67%), $^{12}C_{41}{}^{13}CH_{18}^+$ (29.45%), $^{12}C_{40}{}^{13}C_2H_{18}^+$ (6.75%) and $^{12}C_{39}{}^{13}C_3H_{18}^+$ (1.01%), scale well with their natural abundances. Due to the electron impact ionization, partially H-stripped HBC ions (e.g., $C_{42}H_{16}^+$) are present as well. Peaks at about $m/z$ = 519.2 and 521.3 could in principle also be due to $^{12}C_{42}H_{15}^+$ and $^{12}C_{42}H_{17}^+$. However, as the mass signal ratios are in good agreement with the expected isotopologue values for $^{12}C_{41}{}^{13}CH_{14}^+$ and $^{12}C_{41}{}^{13}CH_{16}^+$, a pure $^{12}C$-based solution is less likely. Hence, in agreement with the laser irradiation experiments to be described below, electron impact ionization leads preferentially to fragmentation losses of 2H (or $H_2$). Also visible in Figure 2A (around $m/z$ = 261) is the doubly-ionized HBC cation $(C_{42}H_{18})^{2+}$. Figure 2A confirms that trapping time and trapping efficiency of i-PoP are very good.

Figure 2B shows the resulting mass spectrum of trapped HBC cations upon 532 nm irradiation at different laser pulse energies where a laser energy of 2.7 mJ corresponds to an average power of $4.5 \times 10^5$ W in the beam. All experiments have the same ion filling time of 3 s and trapped HBC cations are irradiated for similar periods (1.8 s). A wide range of fragment ions are evident in these mass spectra that are attributed to multiple, successive absorption/fragmentation events during the 1.8 s period, as will be discussed in detail below. Figure 2B shows that the terminal photo-fragment pattern clearly depends directly on the incident radiation flux. The general trend that can be observed is that HBC cations dehydrogenate and with increasing laser pulse energy multiple

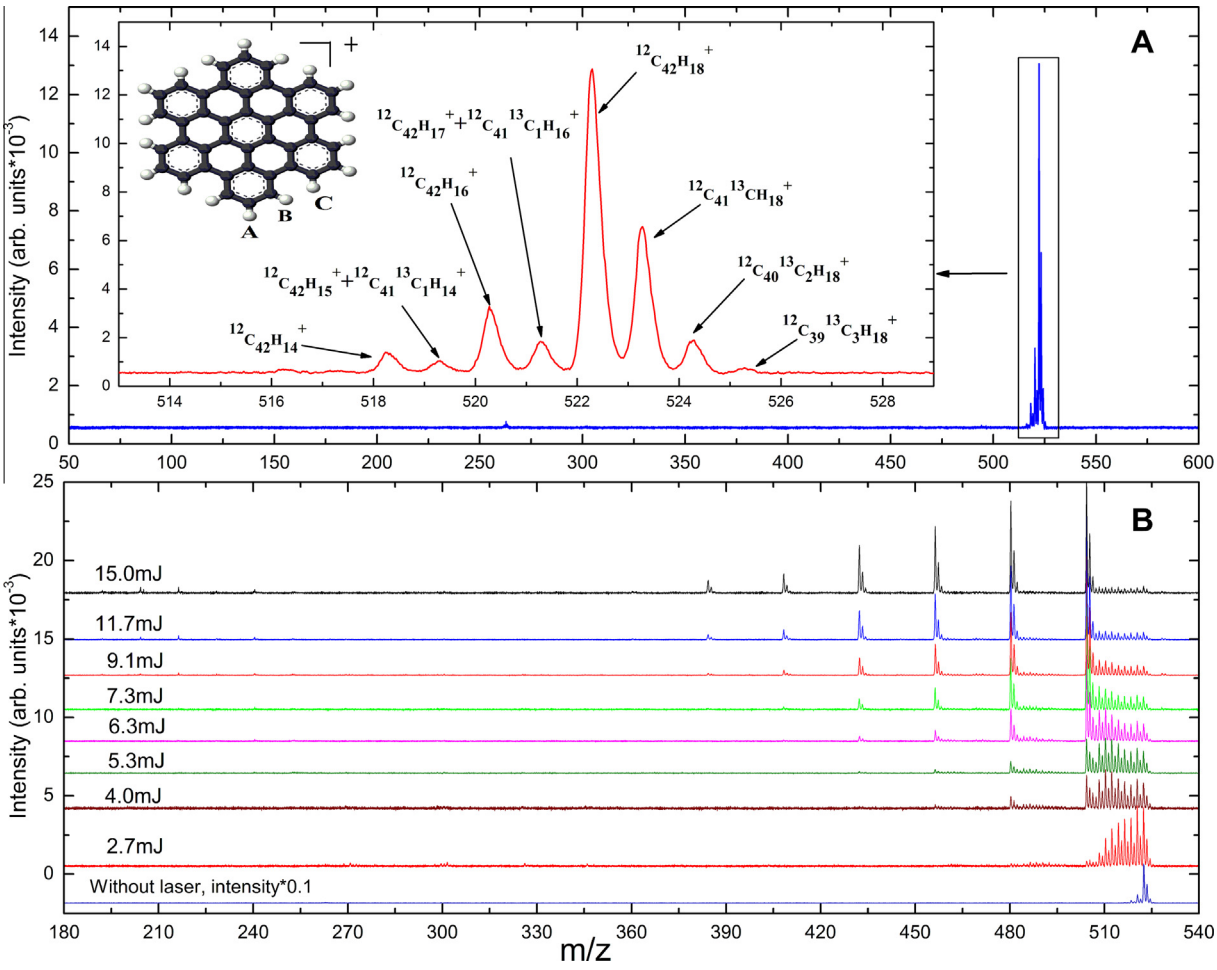


**Figure 2.** Upper panel (A): time-of-flight mass spectrum of the HBC radical cations trapped after evaporation and electron impact ionization. The inset is a zoom-in around $m/z = 522$ revealing the presence of isotopic distribution and dehydrogenated of HBC cations, specifically including 13C-containing species. Lower panel (B): time-of-flight mass spectrum of HBC radical cations irradiated with 532 nm at different laser pulse energies. Note that these mass spectra have been taken after 18 laser pulses and therefore include the effects of irradiation of HBC as well as HBC daughter products during the full measurement cycle.

fragmentation steps become more prominent. In addition, other fragmentation channels become accessible at higher laser pulse energy. For laser pulse energies in the range 2.0–5.0 mJ the photodissociation of HBC mainly follows sequential 2H (or $H_2$) separations, leading to the predominance of even-mass species $^{12}C_{42}H_{2n}^+$ with $n = [0–9]$. Masses corresponding to $C_{30+2*m}H_{2n}^+$ with $m = [0–5]$ and $n = [0–8]$ appear as well, following a $C_2/C_2H_2$-loss channel that has been identified previously as a major fragmentation channel in the dissociation of PAH cations [11,13]. At very high laser pulse energy, the HBC cation can undergo many, many sequential absorption/fragmentation events and it may even lose all of its hydrogen atoms (sequentially) to leave a bare carbon cluster containing 42 carbon atoms. Similar complete dehydrogenation behavior upon laser irradiation has been observed for the small, 24 C-atom coronene and naphtho[2,3-a]pyrene cations [22,24]. Subsequently, $C_{42}^+$ can fragment to smaller pure carbon clusters. This will be discussed later.

More details on the laser pulse energy dependent dissociation behavior are illustrated in Figure 3, in panel A for a lower value and in panel B for a higher value of the laser pulse energy. In panel A, $C_{40}H_{2n}^+$ fragments with $n = [0–8]$ are shown. We corrected the odd H-peak for the $^{13}C$ isotope, taking natural abundances and assuming that the fragmentation pattern is not C-isotope dependent. The dissociation pattern of HBC cation follows the reaction pathways $C_{42}H_{18}^+ \xrightarrow{-nH_2/n(2H)} C_{42}H_{18-2n}^+ \xrightarrow{-mC_2} C_{42-2m}H_{18-2n}^+$ or. $C_{42}H_{18}^+ \xrightarrow{-nC_2H_2} C_{42-2n}H_{18-2n}^+$. The fragment $C_{40}H_4^+$, for example, acts as an intermediate in the dissociation network, as shown in Figure 3A: the production reaction pathways of $C_{40}H_4^+$ are $C_{42}H_6^+ \xrightarrow{-H_2/2H} C_{42}H_4^+ \xrightarrow{C_2} C_{40}H_4^+$ or $C_{42}H_6^+ \xrightarrow{-C_2H_2} C_{40}H_4^+$ and the dissociation reaction pathways of $C_{40}H_4^+$ are $C_{40}H_4^+ \xrightarrow{-H_2/2H} C_{40}H_2^+ \xrightarrow{-C_2} C_{38}H_2^+$ or. $C_{40}H_4^+ \xrightarrow{-C_2H_2} C_{38}H_2^+$ In the 15.0 mJ set of measurements as shown in Figure 3B, all ions are almost completely dehydrogenated, resulting in mass spectra dominated by species with masses in the range of $C_{30}–C_{42}$, and leaving only traces of hydrogenated species, e.g., $C_{42}H_{2n}^+$. The bare carbon clusters that are found mainly originate from $C_{42}^+$ losing $C_2$ fragments. This loss pattern has been observed also for fullerenes [23,25]. However, as we also observe low concentrations of intermediates that have lost one or more $C_2H_2$ groups, as outline above, acetylene-loss with subsequent dehydrogenation may provide an alternative but obviously less important channel for $C_{30}–C_{42}$ formation. Figure 3 also shows low mass fragments in the range $m/z = 180–250$. These peaks may represent the doubly ionized, bare $C_{2n}^{2+}$ clusters with $n = 16–20$. As doubly charged HBC has a very low initial abundance inthese experiments (Figure 2A), any doubly charged cation clusters would involve an additional ionization step. However, thermoionic emission is only observed for systems where the dissociation energy is larger than the ionization potential [28], and with ionization potentials in the range of 10–12 eV and cohesive energies of

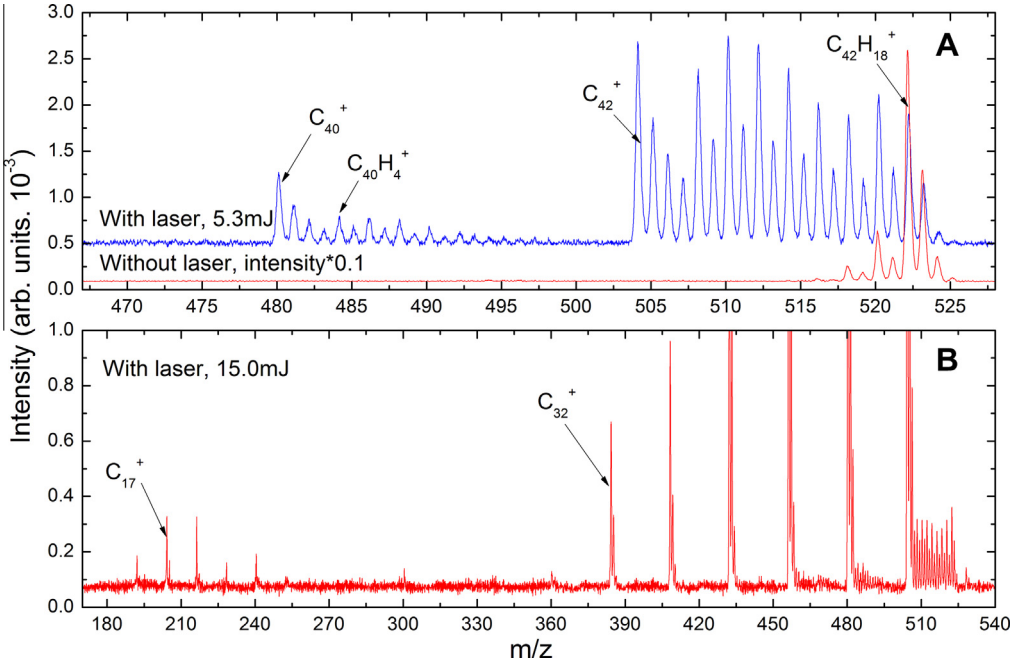


**Figure 3.** Time-of-flight mass spectrum of HBC radical cations: the upper panel (A) is without laser and with 5.3 mJ laser pulse energy; the lower panel (B) is with 15.0 mJ laser pulse energy.

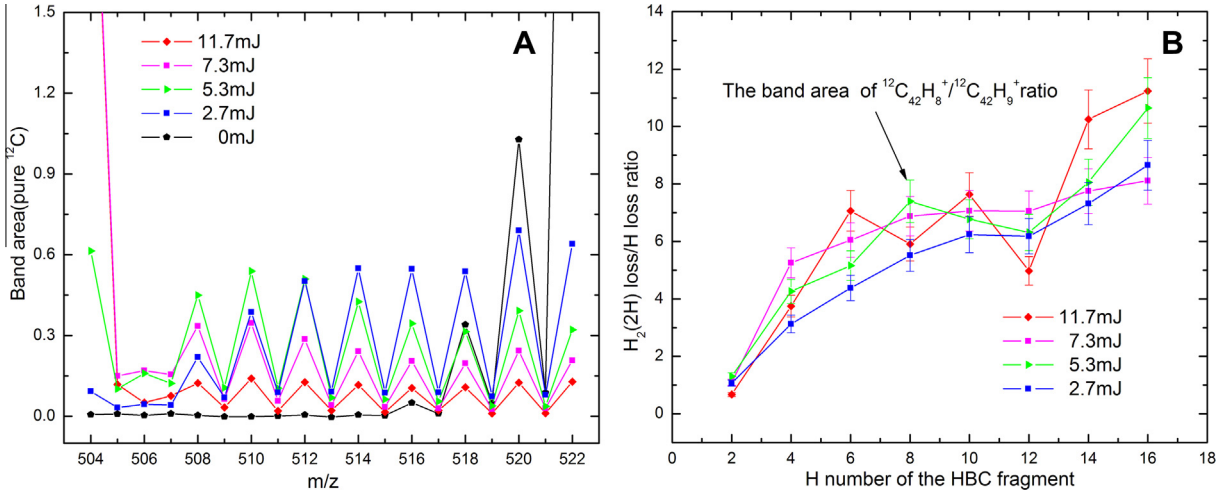


**Figure 4.** The left panel (A) is the calculated value of the integrated signals for the $^{12}C_{42}H_n^+$ (with $n$ = [0–18]) mass peaks, for different laser pulse energies and corrected for the isotope contamination; the right panel (B) shows the ratio of the calculated value of the integrated signals for $^{12}C_{42}H_{2n}^+/^{12}C_{42}H_{2n+1}^+$ with $n$ = [1–8].

6–7 eV for [26,27], depending on cluster size, we consider doubly charged pure carbon clusters highly unlikely candidates for these mass peaks. Rather, as in photo-fragmentation experiments for fullerenes, we recognize the presence of two separate populations of carbon clusters: The first group of pure carbon clusters, $C_n^+$, $n \geqslant 32$, is separated by 2 C-atoms. The second population, $C_n^+$, $n \leqslant 20$, differs by 1 C-atom. In analogy with the fullerenes, it is possible that the first group is carbon cages while the second group may correspond to rings [25]. Follow up studies will have to address the relative importance of fragmentation and isomerization for highly excited, large PAH species.

Given the relatively high abundances of several $^{13}C$ containing HBC isotopologues, the mass spectra should be interpreted with care. Integration and calculations are necessary to obtain the abundances of the pure $^{12}C$ containing species. Starting from the pure $^{12}C_{42}^+$peak, at $m/z$ = 504, higher lying peaks can be corrected for the isotope contaminant using natural abundance values. So, the $m/z$ = 505 peak is corrected for the $^{12}C_{41}{}^{13}C^+$ to derive the abundance of $^{12}C_{42}H^+$. Likewise, mass peak $m/z$ = 506 is corrected for the $^{12}C_{40}{}^{13}C_2^+$ and $^{12}C_{41}{}^{13}CH^+$ to derive the abundance of $^{12}C_{42}H_2^+$, etc. Figure 4A shows the measured values of the integrated signals for $^{12}C_{42}H_n^+$ mass peaks with $n$ = [0–18], for different laser pulse energy and for pure $^{12}C$. This analysis reveals that the even-H/odd-H abundance ratio is very large, and we conclude that mainly cations are produced that have been stripped by one or more $H_2$/(2H)-units. The ratio of $^{12}C_{42}H_{2n}^+/^{12}C_{42}H_{2n+1}^+$ with $n$ = [1–8] (Figure 4B) does not change with laser pulse energy, and this also points towards a common underlying mechanism. The ratio decreases with the number of H left on the HBC fragment. Hence, it seems likely that the internal energy threshold for the H

loss channel and $H_2$/(2H) loss channel becomes more comparable when the number of H left on the HBC fragment decreases. This behavior of the band ratios may reflect the importance of $H_2$ loss or may imply – given the alternating intensity ratio shown in Figure 4 – that loss of the second, sequential H has a substantially lower barrier compared to the loss of the first H.

We have performed complementary DFT calculations (B3LYP/6-31G**), quantitatively characterizing potential fragmentation channels of the HBC cation for different H positions as labeled in the inset of Figure 2A. These results will be described in detail in a separate study [30], but the main findings are mentioned here in support of the interpretation of our measurements. These show an activation energy barrier of 5.89 eV for $H_2$ loss in a bay region ($H_{loc\text{-}B}$ and $H_{loc\text{-}C}$ neighbours in Figure 2A) as compared to 4.72 eV for the first H loss ($H_{loc\text{-}B}$ (in bay H) in Figure 2A) and 3.90 eV for the second H loss ($H_{loc\text{-}A}$ (off bay H, but a direct neigbour of $H_{loc\text{-}B}$) in Figure 2A) that corresponds to the most energetic favorable sequence. The alternative 2H channel loss sequence yields 4.85 eV for the first H loss ($H_{loc\text{-}A}$ in Figure 2A) and 3.77 eV for the second H loss ($H_{loc\text{-}B}$ (in bay H) in Figure 2A). Because of the high symmetry of HBC these processes can take place at different sites. In agreement with earlier DFT calculations for small PAHs, H-loss is governed almost entirely by steric factors and the hydrogens from congested regions of the PAHs are removed preferentially [31]. An experimental study of H-loss for the pyrene cation, ($C_{16}H_{10}^+$) [32] identified separate channels $H_2$ and sequential loss of 2H. At low internal energies, $H_2$ loss dominated despite the higher (derived) Arrhenius energy due to the larger pre-exponential factor reflecting a favorable change in entropy. At high internal energies, loss of 2H dominated. We intend to address the relative importance of these two channels in a future Letter using tunable vacuum UV light as available from synchrotron facilities. For this reason i-PoP has been constructed as a fully mobile system.

In our experiments, HBC becomes highly excited through absorption of multiple photons and Internal Conversion (IC) leaves the molecule highly vibrationally excited in the ground electronic state, typically on a timescale of the order of 50 fs [4,10]. Intramolecular vibrational redistribution (IVR) then quickly equilibrates the excess energy among all available vibrational modes, leaving the cation amenable to renewed excitation through the same electronic system and relaxation sequence. Figure 5 shows the calculated value of the integrated signals for the $^{12}C_{42}H_{18}^+$ radical cations as function of the laser energy in the experiments, the errors of the band area and the laser pulse energy are shown in this figure. During a single pulse multiple photons may be absorbed. For an internal energy of 7.5 eV, corresponding to a microcanonical temperature of ≈1000 K, the cooling between pulses (0.1 s) is approximately 2.3 eV (e.g., the equivalent of one absorbed photon) [4,34,35]. As the internal energy required for fragmentation for HBC is well in excess of this (see below), we will – for simplicity – assume that radiative cooling is unimportant and that HBC

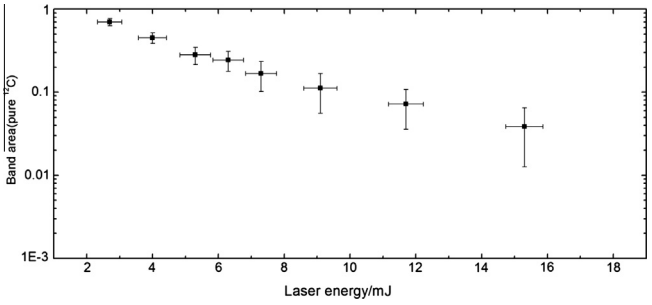


**Figure 5.** The calculated value of the integrated signals for the $^{12}C_{42}H_{18}^+$ radical cations as function of the laser energy in the experiments.

cations that have absorbed at least a critical number of photons, $n_{crit}$, will fragment. The fraction of HBC cations surviving is then given by Poisson statistics and is controlled by the average number of photons absorbed. Adopting the theoretical absorption cross section at 532 nm ($3 \times 10^{-17}$ cm$^2$/molecule) for the HBC cation independent of internal excitation [36], the average number of photons absorbed in a single pulse is equal to (0.30 ± 0.02) photons at a laser pulse energy of 5.0 mJ or 5.4 photons over the experiment. Following [37], this critical number of photons can then be estimated from the experiments by comparing the measured decay curve as a function of laser pulse energy to this simple theoretical model, resulting in $n_{crit} = 4$. The deviation between experiments and the theoretical fit at higher laser pulse energy may reflect the neglect of radiative cooling effects or that the absorption cross section decreases with increasing internal excitation [37]. As an HBC cation starts with ≈0.4 eV of internal energy at 300 K [10], 4 photons corresponds to an internal energy of $E = 9.5$ eV. Following [4,35] we write the dissociation rate in Arrhenius form as,

$$k = k_o \exp[-E_o/k_B T_e] \quad (1)$$

where the effective temperature, $T_e$, is corrected for the finite heat bath and, to a good approximation, can be written for PAHs as [4],

$$T_e = 2000(E(\text{eV})/N_C)^{0.4}(1 - 0.2(E_o(\text{eV})/E(\text{eV}))) \quad (2)$$

Assuming that fragmentation in the experiments implies $k \approx 10\ s^{-1}$ – corresponding to the pulse frequency of 10 Hz – and adopting a pre-exponential factor typical for H-loss from PAHs of $3x10^{16}\ s^{-1}$ [13,29], we arrive at an Arrhenius energy of 3.2 eV, which is then strictly speaking an upper limit. However, a factor 10 higher rate corresponds to an uncertainty of only 0.2 eV in the Arrhenius energy. The derived Arrhenius energy is in good agreement with the results (3.3 eV) [10] derived from an analysis of experiments on H-loss from small PAHs [13]. This is much less than the dissociation energy calculated with DFT (4.72 eV) [30]. Indeed, we note that a barrier of 4.72 eV, would require an internal energy of ≈25 eV for fragmentation on a timescale of 0.1 s, equivalent to $n_{crit} > 10$, and this is clearly excluded by our experiments. This difference is a well-known characteristic when comparing experiments and statistical unimolecular dissociation theories and points towards limitations of unimolecular theory [4].

## 4. Astrophysical relevance

These results and analysis demonstrate that PAH cations offer a molecular reservoir that, upon irradiation, yields a large number of smaller but still complex species. In the ISM, PAHs may form from 'sooting' stars [38,39] and whereas many species discovered in space have been explained as the outcome of reactions involving smaller species, the present Letter is indicative of the importance of a top-down scenario in which molecular transients are due to fragmentation of larger species, specifically PAHs [4,23]. The 'H-atom driven striptease of PAHs' may result in a variety of carbon structures, including carbon sheets, cages, fullerenes, as well as carbon rings and chains [23,25,33]. Given the high radiation fields in the diffuse interstellar medium, it may be interesting to include such species in the discussion of potential carriers of the Diffuse Interstellar Bands [40,41], a family of absorption features generally attributed to large interstellar molecules but whose specific identification has eluded generations of astronomers and spectroscopists [42].

In the ISM, the absorption time-scale is very long and only single photon excitation is generally relevant. The photon energies are limited to 13.6 eV, but higher energy photons are available in regions (e. g., in hot gas, or near O stars). Very close to the star, multiple photons events may also become important. Furthermore,

we recognize that even if the probability for fragmentation in any single event is small, some hundred million absorption events may occur over the lifetime of a PAH molecule in space [4]. Hence, in order to translate the experimental results to conditions relevant to space, the kinetic parameters and the branching ratios involved in the fragmentation steps have to be determined. The present experimental setup, connected to a synchrotron source is well suited to such a systematic study as the energy of the exciting photon can be tuned to 'force' fragmentation of large PAHs (>24 C-atoms) in the 100 μs–100 ms range accessible with our apparatus. Time-resolved fragmentation kinetics would then allow transition state characteristics to be determined [11,32,43].

## 5. Conclusion

We have studied the photo-fragmentation of the HBC cation, $C_{42}H_{18}^{+}$, as the prototypical example of an astrophysically relevant large PAH. Applying 532 nm photolysis, the main fragmentation channels of HBC cations are found for low laser pulse energy to exhibit sequential dehydrogenation followed by $C_2$ ($C_2H_2$) loss. The present data support the idea of a top-down molecular formation scheme in space, starting from PAHs and resulting in a variety of carbon structures, possibly even including graphene [23,24].

## Acknowledgements

We are grateful to M.J.A. Witlox, R. Koehler and J. Grimmerink for technical support, and P. Nash for experimental support. Studies of interstellar chemistry at Leiden Observatory are supported through advanced-ERC Grant 246976 from the European Research Council, through a Grant by the Dutch Science Agency, NWO, as part of the Dutch Astrochemistry Network, and through the Spinoza premie from the Dutch Science Agency, NWO.

## References

[1] L.J. Allamandola, A.G.G.M. Tielens, J.R. Barker, Astrophys. J. 290 (1985) L25.
[2] A. Leger, J.L. Puget, Astron. Astrophys. 137 (1984) L5.
[3] K. Sellgren, Astrophys. J. 277 (1984) 623.
[4] A.G.G.M. Tielens, Ann. Rev. Astron. Astrophys. 46 (2008) 289.
[5] J.D. Bregman, P. Temi, Astrophys. J. 554 (2001) 126.
[6] L.B. Hendecourt, A. Leger, G. Olofsson, W. Schmidt, Astron. Astrophys. 170 (1986) 91.
[7] V.L. Page, T.P. Snow, V.M. Bierbaum, Astron. Astrophys. 584 (2011) 316.
[8] L.J. Allamandola, D.M. Hudgins, S.A. Sandford, Astrophys. J. 511 (1999) L115.
[9] E.L.O. Bakes, A.G.G.M. Tielens, Astrophys. J. 427 (1994) 822.
[10] A.G.G.M. Tielens, The Physics and Chemistry of the Interstellar Medium, Cambridge University Press, 2005.
[11] C. Lifshitz, Int. Rev. Phys. Chem. 16 (1997) 113.
[12] R.C. Dunbar, Int. J. Mass Spectrom. 200 (2000) 571.
[13] H.W. Jochims, E. Ruhl, H. Baumgartel, S. Tobita, S. Leach, Astrophys. J. 420 (1994) 307.
[14] H.W. Jochims, H. Baumgartel, S. Leach, Astrophys. J. 512 (1999) 500.
[15] R.C. Dunbar, C. Lifshitz, J. Chem. Phys. 94 (1991) 3542.
[16] S.P. Ekern, A.G. Marshall, J. Szczepanski, M. Vala, J. Phys. Chem. A 102 (1998) 3498.
[17] G. Rouillé, M. Steglich, F. Huisken, T. Henning, K. Müllen, J. Chem. Phys. 131 (2009) 204311.
[18] D.L. Kokkin et al., Astrophys. J. 681 (2008) L49.
[19] W. Hendel, Z.H. Khan, W. Schmidt, Tetrahedron 42 (1986) 1127.
[20] N.A. Sassin, S.C. Everhart, J.I. Cline, K.M. Ervin, J. Chem. Phys. 128 (2008) 234305.
[21] K. Gulyuz, C.N. Stedwell, D. Wang, N.C. Polfer, Rev. Sci. Instrum. 82 (2011) 54101.
[22] C. Joblin, in: F. Combes et al. (Eds.), SF2A – 2003, Edp. Sci. Conf. Ser., 2003, pp. 175.
[23] O. Berné, A.G.G.M. Tielens, Proc. Natl. Acad. Sci. 109 (2012) 401.
[24] S.P. Ekern, A.G. Marshall, J. Szczepanski, M. Vala, Astrophys. J. 488 (1997) L39.
[25] C. Lifshitz, Int. J. Mass Spectrom. 200 (2000) 423.
[26] G. Seifert, K. Vietze, R. Schmidt, J. Phys. B 29 (1996) 5183.
[27] R.O. Jones, J. Chem. Phys. 110 (1999) 5189.
[28] E.E.B. Campbell, R.R. Levine, Annu. Rev. Phys. Chem. 51 (2000) 65.
[29] V. Le Page, T.P. Snow, V.M. Bierbaum, Astrophys. J. Suppl. 132 (2001) 233.
[30] A. Candian et al. (in preparation).
[31] J. Cioslowski, G. Liu, M. Martinov, P. Piskorz, D. Moncrieff, J. Am. Chem. Soc. 118 (1996) 5261.
[32] Y. Ling, Y. Gotkis, C. Lifshitz, Eur. J. Mass. Spectrom. 1 (1995) 41.
[33] D. Rolland, A.A. Specht, M.W. Blades, J.W. Hepburn, Chem. Phys. Lett. 373 (2003) 292.
[34] P. Boissel, P. Parseval, P. Marty, G. Lefévre, J. Chem. Phys. 106 (1997) 4973.
[35] C.E. Klots, J. Chem. Phys. 90 (1989) 4470.
[36] G. Malloci, C. Joblin, G. Mulas, Astron. Astrophys. 462 (2007) 627.
[37] N.-T. Van-Oanh, J. Phys. Chem. A 110 (2006) 5592.
[38] M. Frenklach, E.D. Feigelson, Astrophys. J. 341 (1989) 372.
[39] I. Cherchneff, PAHs and the Universe, vol. 46, EAS Publications Series, 2011, p. 177.
[40] A.G.G.M. Tielens, Rev. Mod. Phys. 85 (2013) 1021.
[41] M. Steglich, J. Bouwman, F. Huisken, Th. Henning, Astrophys. J. 742 (2011) 2.
[42] N. Cox, J. Cami (Eds.), Proceedings IAU Symposium 297: The diffuse interstellar bands, 2014.
[43] Y. Gotkis, M. Oleinikova, M. Naor, C. Lifshitz, J. Phys. Chem. 97 (1993) 12282.